

The coherent feed-forward loop acts as an efficient information transmitting motif

Md Sorique Aziz Momin,^{*} Ayan Biswas,[†] and Suman K Banik[‡]
Department of Chemistry, Bose Institute, 93/1 A P C Road, Kolkata 700009, India
 (Dated: December 21, 2024)

We present a theoretical formalism to study steady state information transmission in type 1 coherent feed-forward loop motif with an additive signal integration mechanism. Our construct allows a two-step cascade to be slowly transformed into a bifurcation network via a feed-forward loop which is a prominent network motif. Utilizing a Gaussian framework, we show that the feed-forward loop motif harnesses the maximum amount of Shannon mutual information fractions constructed between the input signaling species and the final gene product and also between the two downstream gene products. Our findings may explain why a feed-forward loop is naturally selected by the force of evolution as a motif in bacterial transcription control network while the two-step cascade and bifurcation network are not.

Gene transcription regulatory network (GTRN) is a key player in several physiological processes, e.g., sensory and developmental signaling programs, where it produces gene products some of which are involved in the regulation process itself namely the transcription factors (TFs). TFs are broadly categorized into activators and repressors, the former being involved in up-regulating the expression of its target gene while the latter down-regulate the effector gene. In this fashion, TFs act as the interaction mediators among a number of genes, thus forming several interconnected patterns like cascades, loops etc. The resulting networks have genes as nodes and mainly transcriptional regulation as edges though these may also involve other interactions in post-transcriptional, (post)translational levels [1]. It has been recently found out in experiments supported by theoretical frameworks that this vast chunk of networks is made of simpler building blocks which appear with higher frequencies in a real network than in a random one and with which the nomenclature of ‘network motifs’ has been associated in the literature [2]. These network motifs are abundant in model systems like *E. coli*, *S. cerevisiae*, mouse but also found in humans.

Three nodes interacting with each other generate an ensemble of thirteen distinct patterns or subgraphs of which the only one namely a feed-forward loop (FFL) has been observed to function as a network motif in bacterial GTRN and also in higher organisms [1]. In an FFL, a TF (S) regulates another TF (X) whereas both of them regulate target gene (Y). Depending upon the combinations of activation/repression for the three edges, there arise a total of eight types of FFLs, divided into two major sub-groups. Designating + (−) for activating (repressing) edges, the effective signature of the indirect regulation of Y by S (via X) is determined by the product of two consecutive regulatory signatures (i.e., of $S \rightarrow X$ and $X \rightarrow Y$). If the effective signature of the indirect pathway matches with that of the direct one ($S \rightarrow Y$), FFL is

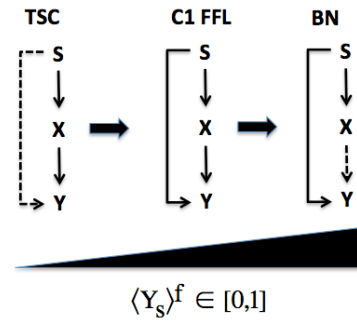


FIG. 1. Schematic diagram depicting the theoretical construct which gradually enables S mediated synthesis of Y ($S \rightarrow Y$ producing $\langle Y_s \rangle$ copies) and consequent disabling of X mediated synthesis of Y ($X \rightarrow Y$ producing $\langle Y_x \rangle$ copies) so that steady state population levels of S, X and Y ($\langle Y \rangle = \langle Y_s \rangle + \langle Y_x \rangle$ copies) remain fixed at each step of topological modifications (Thick arrows). Hence, a TSC is modified into a C1 FFL and finally into a BN. Thin solid (dashed) arrows symbolize presence (absence) of the corresponding genetic interactions. $\langle Y_s \rangle^f =: \langle Y_s \rangle / \langle Y \rangle$ acts as the normalized tuning parameter in our analysis.

of coherent type and incoherent otherwise. Among these eight types, only two are abundant in nature, namely coherent (C) and incoherent (I) type 1 FFL, the former being the model motif of our present analysis [3]. C1 FFL comprises of three activating edges and is utilized in arabinose and flagella system of *E. coli* where input functions similar to AND gate and OR gate is utilized, respectively to integrate activities of upstream TFs (S, X) in the target gene (Y). The former is found to implement a sign-sensitive delay for ON steps [4], while the latter introduces the delay for OFF steps [5] of the signal corresponding to S.

Our present framework is designed to evaluate the effect of topological features of a C1 FFL on its information processing capabilities at steady state. For that purpose, we start from a network pattern where the direct path $S \rightarrow Y$ is absent, and Y is produced entirely from contributions of X via $X \rightarrow Y$. We gradually empower the former edge (contributing $\langle Y_s \rangle$ copies) and correspondingly

^{*} soriqueaziz@jcbose.ac.in
[†] ayanbiswas19@gmail.com
[‡] skbanik@jcbose.ac.in

weaken the latter (contributing $\langle Y_x \rangle$ copies) so that at each of the resulting network configurations, steady state population level of Y ($\langle Y \rangle = \langle Y_s \rangle + \langle Y_x \rangle$) remains fixed. Here, $\langle \dots \rangle$ denotes steady state ensemble average. The edge $S \rightarrow X$ is maintained unaltered with fixed steady state populations of the respective gene products. The two extreme network conformations that we get from our construct are a two-step cascade (TSC), and a bifurcation network (BN) whereas all the intermediate conformations, in principle, falls into the group of C1 FFL (see schematic Fig.1). It is to be noted that neither TSC nor BN is network motif whereas C1 FFL is one. We modeled this genetic motif conforming to a Gaussian framework where gene products S , X , and Y undergo production and degradation (dilution) in a unit effective cellular volume, described neatly in a Langevin formalism. We adopted concepts of information theory to investigate behavioral patterns of key statistical metrics for all the network patterns emerging from our theoretical construct based on which we try to rationalize the evolutionary abundance of an FFL over TSC and BN.

In a C1 FFL, S activates X and both of them activate Y using an additive synthesis mechanism and the resulting dynamics of the copy numbers of S , X , and Y in a unit effective cellular volume can be represented using Langevin formalism as [6–8],

$$\frac{dS}{dt} = f_s - \mu_s S + \xi_s(t), \quad (1a)$$

$$\frac{dX}{dt} = f_x(S) - \mu_x X + \xi_x(t), \quad (1b)$$

$$\frac{dY}{dt} = f_y(S, X) - \mu_y Y + \xi_y(t). \quad (1c)$$

The synthesis rates are $f_s = k_s$ for $\varphi \rightarrow S$, $f_x = k_{sx}(S^n/(S^n + K_{sx}^n))$ for $S \rightarrow X$, $f_y = k_{sy}(S^n/(S^n + K_{sy}^n)) + k_{xy}(X^n/(X^n + K_{xy}^n))$ for $S \rightarrow Y$ Add $X \rightarrow Y$ [9]. k and μ are the synthesis and degradation rate parameters whereas the Hill function ($S^n/(S^n + K_{sx}^n)$) denotes the occupancy probability of promoter in gene X by S with cooperativity index n and activation coefficient K_{sx} for the transcriptional event $S \rightarrow X$ and so on. Noise terms ($\xi_i, i = s, x, \text{ and } y$) are modeled as independent white Gaussian type with $\langle \xi_i(t) \rangle = 0$ and $\langle \xi_i(t) \xi_j(t') \rangle = \langle |\xi_i|^2 \rangle \delta_{ij} \delta(t - t')$ [10]. $\langle \dots \rangle$ is used to denote steady state ensemble average. Noise strengths are generated equally from synthesis and degradation of the biochemical species at steady state. For species S , it is expressed as $\langle |\xi_s|^2 \rangle = \langle f_s \rangle + \mu_s \langle S \rangle = 2\langle f_s \rangle (= 2\mu_s \langle S \rangle)$, which is an approximation. Steady state noise strengths for X and Y are modeled similarly. Taking recourse to the linear noise approximation (LNA) [11, 12] and Lyapunov equation at steady state [13, 14] we arrive at the set of closed form analytic expressions for the Gaussian random variables representing the three gene products (see Eqns.(S2-S7) of the supplemental material).

Information theory established by Claude Shannon [15], has been used in recent years to deal with signal processing in biological systems primarily in neuro-

science perspective [16–18]. One particular information-theoretic approach to understand the biological phenomenon is Ref. [19] where mutual information (MI) between input signals and output response in *V. harveyi* quorum-sensing network was quantified. The network structure used by this model of the marine bacterium to process incoming autoinducer signals is of a converging (integrating) type similar to the FFL motif. Applications to other biochemical networks also made significant contributions making accurate predictions regarding developmental processes in fruit fly embryo [20]; others linked network topology with information processing capabilities [21, 22] whereas research was also directed to estimate the effect of various noise sources in a cellular population on its transmitted information content [23]. Information theory has also been used interfacing with experiments on yeast TF *Msn2* to find high fidelity information transduction of signal identity in contrast with signal intensity [24]. Previous studies also shed light on information-theoretic connotations of biological fitness [22, 25]. Another important study focussed on information optimization in a genetic non-loop feed-forward pattern [26]. In Ref. [27], the FFL has been shown to act as filters when exposed to temporally varying signals.

The inherent stochastic behavior of the biochemical species can be quantified using the concept of entropy of the associated random variables. In other words, the entropy of a gene product quantifies the extent of its uncertainty or fluctuations. The inter-specific coupling of two gene products makes their individual (marginal) entropy spaces to overlap with each other, the common or shared region denoting the MI between them. MI is symmetric with respect to its argument variables. MI denotes how much uncertainty of a gene product can be reduced on average if knowledge of another gene product is available and vice versa [28, 29]. This concept is readily generalizable to include three variables where one quantifies how much fluctuation space a particular random variable shares with a group of two other random variables. For pictorial depiction of MI, we refer our readers to the Venn diagrams in supplemental Figs.(S1-S3). For Gaussian random variables, MI is expressible as a logarithmic functional of second moments e.g., MI constituted between S and Y is $I(S; Y) = (1/2) \log_2(\Sigma(S)/\Sigma(S|Y))$ in the units of ‘bits’. Here, $\Sigma(S)$ and $\Sigma(S|Y)$ are the variance of S and partial variance of S conditioned on Y . Analogously, three-variable MI between S and (X, Y) is expressed as $I(S; X, Y) = (1/2) \log_2(\Sigma(S)/\Sigma(S|X, Y))$ [30]. $\Sigma(S|X, Y)$ is computed by conditioning on X and Y . For the formulae of partial variances, we refer to Eqs. (S8-S9) of the supplemental material. Permuting the status of S , X , and Y as the information sources and target, we can arrive at other three-variable MI, e.g., $I(X; Y, S)$.

We increase k_{sy} so as to increase $\langle Y_s \rangle$ by 1 copy at an instant and also decrease k_{xy} and consequently $\langle Y_x \rangle$ by an equal amount so that $\langle Y \rangle$ remains fixed at 100 copies in a unit effective cellular volume. Thus, the direct transcriptional edge $S \rightarrow Y$ is gradually strengthened and

indirect transcriptional edge $X \rightarrow Y$ is equally weakened. $\langle S \rangle = 10, \langle X \rangle = 100$ copies are also maintained throughout the entire process. Keeping gene expression levels fixed while the three-node topology in perspective is discretely modified, helps to compare different network architectures on an equal footing [1]. Whenever the construct allows signal S and X to converge onto Y , this takes recourse to an additive integration mechanism. We start with $k_{SY} = 0$ (k_{XY} maximum) that makes $\langle Y_S \rangle = 0$ ($\langle Y_X \rangle = \langle Y \rangle$) and the resulting network is a TSC, $S \rightarrow X \rightarrow Y$. Here, the signal from first level TF i.e., S is relayed to final gene product Y via an intermediate level TF i.e., X . TSC is typically found in transcriptional networks engaged in slow and irreversible processes like developmental phenomena in *sea urchin*, *D. melanogaster* etc [31]. The other end where k_{SY} is maximum ($k_{XY} = 0$) i.e., $\langle Y_S \rangle = \langle Y \rangle$ ($\langle Y_X \rangle = 0$) is a BN. In a BN, S activates two of its downstream gene products X and Y which do not have any direct interaction between them. BN is composed of two one-step cascade (OSC) namely, $S \rightarrow X$ and $S \rightarrow Y$. OSC is important for sensory signal transduction which is supposed to be fast and reversible [31]. All the intermediate operating points for which $\langle Y_S \rangle$ ($\langle Y_X \rangle$) = 1 - 99 copies, designate to C1 FFL where S activates the synthesis of X and both of them activates production of final gene product Y . In other words, both the direct and indirect regulatory branches contribute (at least 1 copy) in production of Y , which always maintains a constant pool of 100 copies in a unit effective cellular volume. The entire range of $\langle Y_S \rangle^f$ ($\langle Y_S \rangle^f =: \langle Y_S \rangle / \langle Y \rangle$) keeps the genetic identities of S and Y (a regulatory input and a target gene product, respectively) same throughout but not for X which is an intermediate TF in both TSC and FFL but in BN it is one of the effector gene products, another being Y . Therefore in TSC, X and Y are the encoded and decoded signal, respectively. FFL also treats X as an encoded signal whereas Y is the culmination of direct decoding ($\langle Y_S \rangle$) and indirect decoding ($\langle Y_X \rangle$) of input S . In a BN, both X and Y cherish the status of the direct decoded signal via two OSCs. The correlation developed between X and Y in a BN is thus completely assisted by the fluctuation space of S . TSC have been found to operationalize synergistic and redundant information in its embedded information channels [6, 8]. On the other hand, BN may work as an upper-level sub-motif creating information redundancy in a diamond motif which is a variant of FFL with duplication of intermediate gene X [7].

The inter-genetic interactions among S , X , and Y being essentially nonlinear augmented by cooperative binding of TF molecules to their target promoter sites, the correlation structure is suitably quantified using MI rather than simple linear measures, e.g., Pearson correlation coefficient. Taking into consideration all the three different types of network manifestations coming out of our theoretical construct, it can be generally stated that $I(S;Y)$ is the overlap between entropy spaces of the first-level signaling TF S and the utmost downstream (one of the

two in case of BN) gene product Y . Similarly, $I(X;Y)$ is the shared proportion of entropic contributions of two downstream gene products X (activator in TSC and FFL) and Y (effector gene product). $I(S;X,Y)$ is $I(S;Y)$ added with MI of S and X given the knowledge of Y , i.e., $I(S;X|Y)$. Similarly, adding MI between X and S given the knowledge about Y , i.e., $I(X;S|Y)$ ($= I(S;X|Y)$) to $I(X;Y)$ amounts to a production of $I(X;Y,S)$. These MI terms are related to each other forming chain rules [28, 29]

$$I(S; X, Y) = I(S; Y) + I(S; X|Y), \quad (2a)$$

$$I(X; Y, S) = I(X; Y) + I(X; S|Y). \quad (2b)$$

In this communication, our objective is to measure the strength of these two-variable MI with respect to corresponding three-variable total MI as the output gene product Y is gradually enabled to sense S directly thereby gradually becoming independent of X .

Fig. 2(a-b) includes the profiles of several MI normalized by their respective maximum value (denoted by superscript 'N'), thereby showing their nature of variations subject to changing $\langle Y_S \rangle^f$. As the contributions of direct path (indirect path) increases (decreases), $I^N(S; Y)$ ($I^N(X; Y)$) grows (decays) in Fig. 2(a). These trends are also manifested for normalized three-variable MI, $I^N(S; X, Y)$ and $I^N(X; Y, S)$ in Fig. 2(b). Since the MI captures in it the fluctuations associated with its argument random variables, we dissected $\Sigma(Y)$ into its constituents which involve separate contributions from the direct OSC ($S \rightarrow Y$) and the indirect TSC ($S \rightarrow X \rightarrow Y$) pathways as well as a cross term (CT) incorporating both of them and therefore,

$$\Sigma(Y) = \Sigma(Y)_{\text{OSC}} + \Sigma(Y)_{\text{TSC}} + \Sigma(Y)_{\text{CT}}. \quad (3)$$

For the analytic expressions of these contributions readers are referred to consult Eqns. (S10-S12) in the supplemental material. Fig. 2(c) portrays these expressions normalized by their respective maximum value. While $\Sigma(Y)_{\text{OSC}}^N$ has a growing nature, $\Sigma(Y)_{\text{TSC}}^N$ decays whereas the profile of $\Sigma(Y)_{\text{CT}}^N$ is concave down. These observations can be justified by noting that $\Sigma(Y)_{\text{OSC}}^N \propto \langle Y_S \rangle + c_1 \langle Y_S \rangle^2$, $\Sigma(Y)_{\text{TSC}}^N \propto \langle Y_X \rangle + c_2 \langle Y_X \rangle^2$, and $\Sigma(Y)_{\text{CT}}^N \propto c_3 \langle Y_S \rangle \langle Y_X \rangle$, where c_1 , c_2 , and c_3 are constants determined by network parameters. The individual MI terms do not distinguish FFL and the same can be said for $\Sigma(Y)_{\text{OSC}}^N$ and $\Sigma(Y)_{\text{TSC}}^N$. $\Sigma(Y)_{\text{CT}}^N$ is maximum where $\langle Y_S \rangle^f = 0.5$ i.e., both the direct and the indirect branch of FFL contributes equally. These observations lead us to search for suitable multivariate information-theoretic metric which can provide insights for the FFL topology. To this end, we define two rescaled metrics

$$I^f(S; Y) =: I(S; Y) / I(S; X, Y), \quad (4a)$$

$$I^f(X; Y) =: I(X; Y) / I(X; Y, S). \quad (4b)$$

Fig. 3(a) depicts $I^f(S; Y)$ and $I^f(X; Y)$ and both of them are ≈ 1 for an extended regime of $\langle Y_S \rangle^f$ that takes

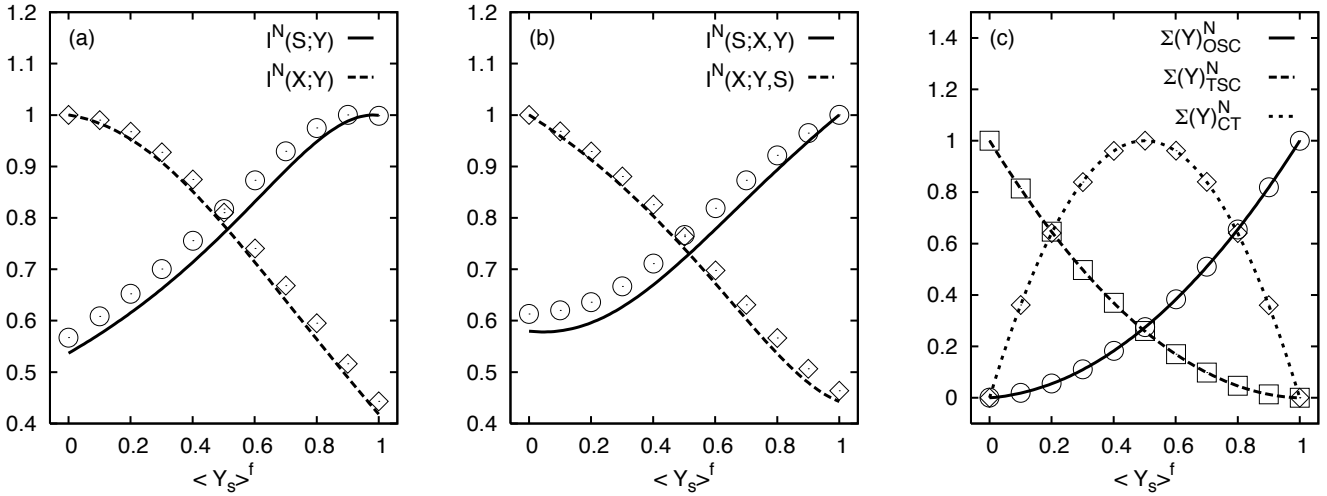


FIG. 2. (a) Two-variable MI, $I(S;Y)$ and $I(X;Y)$ normalized by their respective maximum value, producing $I^N(S;Y)$ and $I^N(X;Y)$, respectively. Similarly, (b) normalized three-variable MI, $I^N(S;X,Y)$ and $I^N(X;Y,S)$, and (c) normalized constituents of $\Sigma(Y)$ i.e., $\Sigma(Y)_{OSC}^N$, $\Sigma(Y)_{TSC}^N$, and $\Sigma(Y)_{CT}^N$. The horizontal axis represents $\langle Y_s \rangle^f$. As the edge $S \rightarrow Y$ ($X \rightarrow Y$) is gradually enabled (disabled) as a result of which, $\langle Y_s \rangle^f$ ($\langle Y_x \rangle^f$) increases (decreases); $I^N(S;Y)$ and $I^N(S;X,Y)$ ($I^N(X;Y)$ and $I^N(X;Y,S)$) increases (decreases). One striking feature is the cross over regime between $I^N(S;Y)$ and $I^N(X;Y)$ and also between $I^N(S;X,Y)$ and $I^N(X;Y,S)$, occurring when strengths of both $S \rightarrow Y$ and $X \rightarrow Y$ are approximately equal and therefore $\langle Y_s \rangle^f \approx 0.5 \approx \langle Y_x \rangle^f$. $\Sigma(Y)_{OSC}^N$ and $\Sigma(Y)_{TSC}^N$ intersect each other and the peak of $\Sigma(Y)_{CT}^N$ appears exactly at $\langle Y_s \rangle^f = 0.5 = \langle Y_x \rangle^f$. Population levels are fixed at $\langle S \rangle = 10$, $\langle X \rangle = 100$, and $\langle Y \rangle = 100$ all in the units of copy per unit effective cellular volume. Relaxation rate parameters are $\mu_s = 0.1$, $\mu_x = 0.5$, and $\mu_y = 5.0$ all in the units of min^{-1} . Synthesis rate parameters are determined according to $k_s = \mu_s \langle S \rangle$, $k_{sx} = \mu_x \langle X \rangle (\langle S \rangle^n / (\langle S \rangle^n + K_{sx}^n))^{-1}$, $k_{sy} = \mu_y \langle Y_s \rangle (\langle S \rangle^n / (\langle S \rangle^n + K_{sy}^n))^{-1}$, and $k_{xy} = \mu_y \langle Y_x \rangle (\langle X \rangle^n / (\langle X \rangle^n + K_{xy}^n))^{-1}$. Here, Hill coefficient $n = 2$ and activation coefficients are $K_{sx} = \langle S \rangle$, $K_{sy} = \langle S \rangle$, and $K_{xy} = 2\langle X \rangle$. These parameters effectively make the occupancy probability of promoter Y by X , 0.2 which is characteristic of linear activation whereas other regulatory edges employ half maximal activation. Lines are drawn using analytical results obtained from LNA. These are supported by *in silico* results obtained by averaging over ensemble of 10^5 independent samples derived from Gillespie SSA [32, 33] and are drawn as symbols.

into account active participation of both direct and indirect branches within C1 FFL. The inset of Fig. 3(a) shows $\Sigma(Y)_{CT}^f (= \Sigma(Y)_{CT} / \Sigma(Y)_{FFL})$ which peaks inside the extended parametric regime of a C1 FFL. TSC and BN provide lesser values for all of these metrics. This gives a quantitative understanding of the network structure where two-variable MI becomes sufficient to replace the corresponding three-variable total MI. The parameters for which both $\langle Y_s \rangle$ and $\langle Y_x \rangle$ become significant, lead to form a C1 FFL motif with moderately strong direct and indirect pathways. The portion of the information content of S , which is filtered out depending upon the separation of relaxation time scales between S and X , now gets an alternative route to bypass X and directly feed gene Y . Our present construct sets $\mu_x = 5\mu_s$ whereas $\mu_y = 50\mu_s$ which enables Y to sample S much better than what X does. The FFL region showing $I^f(S;Y) \approx 1$ signifies $I(S;Y) \approx I(S;X,Y)$ according to Eqn. (4a). The relevance of X is consequently diminished as uncertainty reduction of S using X becomes minimal. This gets reflected in $I^f(S;X|Y) \approx 0$ where the fraction is taken with respect to $I(S;X,Y)$ (see Fig.3(b)). Since $I(S;X,Y)$ is finite, this means $I(S;X|Y) \approx 0$ (see

Eqn. (2a)) indicative of an approximate Markov chain $S \rightarrow Y \rightarrow X$ i.e., S and X are conditionally independent of each other provided Y is known [28]. Interestingly enough, this parametric domain also contributes maximum $I^f(X;Y)$ (≈ 1) implying $I(X;Y) \approx I(X;Y,S)$ following Eqn. (4b). In this FFL region, $I^f(X;Y)$ practically overlaps with $I^f(S;Y)$. Correspondingly in Fig.3(b), we note that $I(X;S|Y) \approx 0$, i.e., there exists another approximate Markov chain $X \rightarrow Y \rightarrow S$.

In this communication, we presented an information-theoretic framework which allows to distinguish a C1 FFL from a TSC and BN and put forward a hypothesis that rationalizes the abundance of the former than the latter two patterns. Our findings show that neither two nor three-variable MI directly provides any advantage point for FFL, but fractions of the two-variable MI with respect to the total three-variable MI may possibly provide a hint in this direction. The set of biologically plausible parameters in our model provides maximal MI fractions for an extended region where both the direct and indirect branches of the FFL are reasonably well functional in synthesizing the target gene product. The parameter for which the interference between these

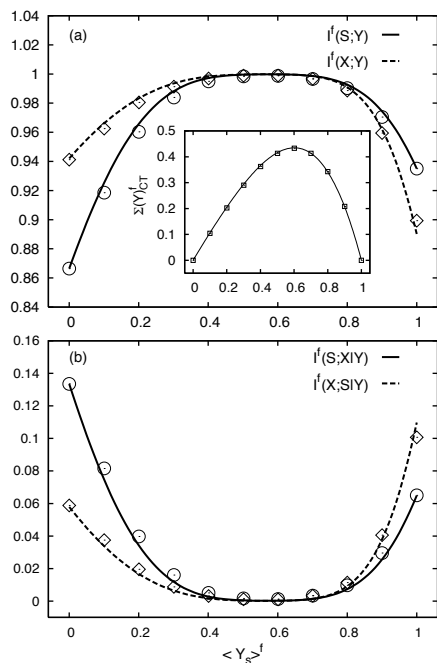


FIG. 3. (a) $I^f(S;Y)$, $I^f(X;Y)$ and $\Sigma(Y)_{CT}^f$ (inset), (b) $I^f(S;X|Y)$, $I^f(X;S|Y)$ with respect to $\langle Y_s \rangle^f$. In panel (a), we find that parameters belonging to a C1 FFL provide maximum amount of $I^f(S;Y)$, $I^f(X;Y)$ (≈ 1) than the TSC and BN, thereby forming a plateau. $\Sigma(Y)_{CT}^f$ is a functional of both $\langle Y_s \rangle$ and $\langle Y_x \rangle$ (see supplemental text) and peaks while the three-node network passes through parametric region belonging to the FFL. In panel (b), partial MI fractions show antagonistic nature to profiles of previous MI fraction in panel (a). Here, analytical results are shown with lines. Accompanying simulation data (average of 10^5 independent time series) using Gillespie SSA are denoted by symbols. Parameters used are similar to that of Fig. 2.

two branches produces maximum fluctuations in the target gene product also falls in this extended parametric regime. This efficient FFL domain is marked by two approximate markov chains $S \rightsquigarrow Y \rightsquigarrow X$ and $X \rightsquigarrow Y \rightsquigarrow S$ which imply knowing (conditioning on) Y makes entropy spaces of S and X mutually exclusive to each other. The two extreme points corresponding to $\langle Y_s \rangle^f = 0, 1$ denote

pure TSC and BN, respectively. For a TSC, $S \rightarrow X$ can be thought of as an encoding step for information coming from S and stochastically manifested in X , whereas $X \rightarrow Y$ is the decoding step which retrieves the encoded message and the transcriptional program ends with synthesis of Y . For an FFL, there is an additional decoding route $S \rightarrow Y$, which evades the intermediate encoder X . In a BN, indirect decoding is absent as the edge between X and Y is non-existent. Hence, TSC correlates S and Y via X , whereas BN has a direct correlation between them. On the other side, X and Y are directly correlated in TSC, but in BN, it is all controlled by the fluctuation space of S . FFL benefits from utilizing both direct and indirect decoding of upstream signal S , thereby better coordinating the transcriptional program as a response to environmental stimuli. The biological meaning behind the concepts of three-variable MI is also interesting to understand this encoding-decoding mechanism in FFL. In an FFL, to diminish the uncertainty about S beyond what is already done by X , the remaining gene product Y may also be utilized, and therefore $I(S;X;Y)$ enters the quantitative domain. The same logic applies for constructing $I(X;Y;S)$ as we further access the input TF (S) along with Y to have a better knowledge of intermediate TF (X). Our analysis has pointed out that the ratio of two-variable and three-variable MI may possibly be a better candidate measure to evaluate the decoding mechanism in C1 FFL, whereas individual MI terms fail to do so. The metric proposed by us clearly shows that C1 FFL outperforms TSC and BN, in the capacity of an efficient decoder of environmental signal. This physical principle of maximal decoding capacity may be one of the possible reasons behind natural selection of C1 FFL as a network motif in contrast with TSC and BN. Our predictions can be directly tested in synthetic bacterial circuitries. *In vivo*, C1 FFL may be embedded in larger networks involving feedback and auto-regulation, and it would be interesting to check whether our present framework remains tenable, taking into account these additional interactions.

Md SAM is supported by DST, Govt. of India, through INSPIRE research fellowship (DST/INSPIRE Fellowship/2018/IF180056). AB and SKB acknowledges Bose Institute, Kolkata for research support.

-
- [1] U. Alon, *An Introduction to Systems Biology: Design Principles of Biological Circuits* (CRC Press, Boca Raton, 2006).
 - [2] R. Milo, S. Shen-Orr, S. Itzkovitz, N. Kashtan, D. Chklovskii, and U. Alon, *Science* **298**, 824 (2002).
 - [3] S. Mangan and U. Alon, *Proc. Natl. Acad. Sci. U.S.A.* **100**, 11980 (2003).
 - [4] S. Mangan, A. Zaslaver, and U. Alon, *J. Mol. Biol.* **334**, 197 (2003).
 - [5] S. Kalir and U. Alon, *Cell* **117**, 713 (2004).
 - [6] A. Biswas and S. K. Banik, *Phys. Rev. E* **93**, 052422 (2016).
 - [7] A. Biswas and S. K. Banik, *Chaos* **28**, 103102 (2018).
 - [8] A. Biswas, *Chaos* **29**, 063108 (2019).
 - [9] L. Bintu, N. E. Buchler, H. G. Garcia, U. Gerland, T. Hwa, J. Kondev, and R. Phillips, *Curr. Opin. Genet. Dev.* **15**, 116 (2005).
 - [10] F. Tostevin and P. R. ten Wolde, *Phys. Rev. E* **81**, 061917 (2010).
 - [11] N. G. van Kampen, *Stochastic Processes in Physics and*

- Chemistry, 3rd ed.* (North-Holland, Amsterdam, 2007).
- [12] J. Elf and M. Ehrenberg, *Genome Res.* **13**, 2475 (2003).
- [13] J. Paulsson, *Nature* **427**, 415 (2004).
- [14] J. Paulsson, *Phys Life Rev* **2**, 157 (2005).
- [15] C. E. Shannon, *Bell. Syst. Tech. J* **27**, 379 (1948).
- [16] A. Borst and F. E. Theunissen, *Nat. Neurosci.* **2**, 947 (1999).
- [17] N. Timme, W. Alford, B. Flecker, and J. M. Beggs, *J Comput Neurosci* **36**, 119 (2014).
- [18] N. M. Timme and C. Lapish, *eNeuro* **5**, 0052 (2018).
- [19] P. Mehta, S. Goyal, T. Long, B. L. Bassler, and N. S. Wingreen, *Mol. Syst. Biol.* **5**, 325 (2009).
- [20] W. Bialek, *Biophysics: Searching for principles* (Princeton University Press, Princeton, 2012).
- [21] R. Cheong, A. Rhee, C. J. Wang, I. Nemenman, and A. Levchenko, *Science* **334**, 354 (2011).
- [22] A. Tareen, N. S. Wingreen, and R. Mukhopadhyay, *Phys Rev E* **97**, 020402 (2018).
- [23] M. Chevalier, O. Venturelli, and H. El-Samad, *PLoS Comput. Biol.* **11**, e1004462 (2015).
- [24] A. S. Hansen and E. K. O'Shea, *eLife* **4**, e06559 (2015).
- [25] S. F. Taylor, N. Tishby, and W. Bialek, arXiv:0712.4382v1 [q-bio.PE] (2007).
- [26] A. M. Walczak, G. Tkačik, and W. Bialek, *Phys. Rev. E* **81**, 041905 (2010).
- [27] W. H. de Ronde, F. Tostevin, and P. R. ten Wolde, *Phys. Rev. E* **86**, 021913 (2012).
- [28] T. M. Cover and J. A. Thomas, *Elements of Information Theory* (Wiley-Interscience, New York, 1991).
- [29] D. J. C. MacKay, *Information Theory, Inference & Learning Algorithms* (Cambridge University Press, New York, 2002).
- [30] A. B. Barrett, *Phys. Rev. E* **91**, 052802 (2015).
- [31] N. Rosenfeld and U. Alon, *J. Mol. Biol.* **329**, 645 (2003).
- [32] D. T. Gillespie, *J. Comp. Phys.* **22**, 403 (1976).
- [33] D. T. Gillespie, *J. Phys. Chem.* **81**, 2340 (1977).